Nanomechanical and Electrochemical Properties of ZnO-Nanoparticle-Filled Epoxy Coatings

Ubair Abdus Samad [1], **Mohammad Asif Alam** [1,*], **Arfat Anis** [2,*], **Hany S. Abdo** [1], **Hamid Shaikh** [2] **and Saeed M. Al-Zahrani** [2]

1 Center of Excellence for Research in Engineering Materials (CEREM), King Saud University, P.O. Box 800, Riyadh 11421, Saudi Arabia; uabdussamad@ksu.edu.sa (U.A.S.); habdo@ksu.edu.sa (H.S.A.)
2 SABIC Polymer Research Center (SPRC), Chemical Engineering Department, King Saud University, P.O. Box 800, Riyadh 11421, Saudi Arabia; hamshaikh@ksu.edu.sa (H.S.); szahrani@ksu.edu.sa (S.M.A.-Z.)
* Correspondence: moalam@ksu.edu.sa (M.A.A.); aarfat@ksu.edu.sa (A.A.)

Abstract: This work focuses on the mechanical, nanomechanical, thermal, and electrochemical properties of epoxy coatings with various percentages of ZnO nanoparticles. The prepared coatings were analyzed after complete curing of 7 days. The dispersion of nanoparticles in the matrix was analyzed by Scanning Electron Microscopy (SEM) followed by Fourier-Transformed Infrared Spectroscopy (FTIR) to evaluate the effect of the nanoparticles on curing and Differential Scanning Calorimetry (DSC) to evaluate its thermal properties. The electrochemical (anticorrosion) properties of the coatings were analyzed by exposing the prepared coatings to a 3.5% NaCl solution. The obtained results indicated that the addition of the nanoparticles was effective at lower loadings; higher loadings of the nanoparticles led to increased agglomeration because of higher particle–particle interaction. At higher nanoparticle loadings, the curing process was adversely affected, which led to lower curing percentage. The lower degree of curing affected the thermal, mechanical, and electrochemical properties. The increase in nanoparticle loading beyond 2% negatively affected the coating properties.

Keywords: epoxy coating; nanoparticles; zinc oxide; corrosion; nanoindentation; mechanical properties; thermal properties

1. Introduction

Corrosion is a naturally occurring phenomenon that causes huge economic implications globally, which according to an estimate costs over 3% of the world's GDP. Hence, corrosion itself and the steps taken for its reduction and prevention are a very crucial subject. The corrosion prevention of metals that are widely used in different aspects of life such as automotive and other heavy industries is usually performed by various approaches [1]. Among various types of methods, the use of organic coatings is at the center of importance. Organic coatings are the most feasible and important economical method to be used for corrosion prevention [2]. Irrespective of their lower thickness, these organic coatings act as a resistance against water and other corrosive species present in the aggressive medium that causes corrosion. These coatings are also termed as barrier coatings because they provide barrier against corrosion and protect the metal's surface.

With the rising use of various types of organic coatings, epoxies are usually considered the most promising candidate because of the offered advantages and their ease of use for different types of applications. The use of epoxy as a coating material offers many benefits such as mechanical strength, thermal resistance, and great adhesion to various types of substrates. On the other hand, use of epoxy has some shortcomings as well, such as lower long-term corrosion prevention because of poor long-term resistance against water permeability and corrosive agents [3]. The poor weathering properties of epoxy also limit

their use in outdoor applications where the exposure to UV light harms the properties and causes failure [4,5].

Currently, nanotechnology has become the core participant in order to improve the materials' performance and properties by many fold. The inclusion of nanoparticles in the coatings is proving to be helpful in terms of performance compared to neat polymer coatings [6]. These nanoparticles provide superior properties to conventional micro-sized fillers even at smaller concentrations [7,8]. The main factor in achieving enhanced properties with the utilization of nanoparticles is their homogenous dispersion. The nanoparticles, because of their higher surface area, are more prone to interact with each other and tend to agglomerate [9]. The use of different nanosized fillers results in the creation of material that possess excellent properties, which can be utilized in a vast range of applications. In order to promote the use of polymer coatings, several nanotechnology-based attempts have been made specifically related to outdoor performance [10–15]. In the literature, numerous research works have highlighted the use of ZrO_2, ZnO, and TiO_2 nanoparticles in order to achieve a higher performance of polymeric nanocomposites, and they are even used to enhance the polymeric coating's performance [10,16–21]. Rashvand et al. [10] investigated the use of ZnO as a UV-stabilizer in an aromatic polyurethane coating system using the cathodic electrodeposition process. They found that ZnO reduced the polyurethane's photo degradation and also prevented the yellowing of the film. Sorkhabi et al. [22] synthesized ZnO nanoparticles using the precipitation method, and these nanoparticles were then added to epoxy (0.1 wt.%, 1 wt.%, and 10 wt.%) and coated via the dipping method. They reported an increase in the anticorrosion properties of the coatings at lower concentrations of ZnO. Ammar et al. [23] prepared epoxy polydimethylsiloxane composite coatings with different percentages of ZnO nanoparticles (2–8 w/w) with the help of the solution intercalation method. They reported an increase in the corrosion resistance of the coatings with a 2 w/w ratio of nanoparticles in epoxy; they also reported an increase in hydrophobicity of the coatings with 6 w/w%. Parimalam et al. [24] prepared hybrid epoxy coatings by incorporating different fillers including ZnO in the coatings. The results revealed that the addition of TiO_2 and ZnO resulted in better UV radiation resistance, while the presence of SiO_2 enhanced the chemical resistance of the coatings. The use of nanoparticles in improving the anticorrosion properties of polymer coatings has been of great importance. This is because the diffusion paths for corrosive species in the presence of nanoparticles is much longer than coatings without nanoparticles. Hence, these organic coatings with nanoparticles exhibit better anti-corrosion properties than pure polymer coatings [25].

In the following work, we focused on the use of ZnO nanoparticles as high as 6 wt.% in the epoxy system to analyze the effect of the nanoparticles on the final properties of the coatings. The evaluation of the dispersion of the nanoparticles was performed with the help of a Field Emission Scanning Electron Microscope (FE-SEM, JEOL, Tokyo, Japan). The thermal properties such as the glass transition temperature (Tg) of the prepared coatings were evaluated using Differential Scanning Calorimetry (DSC, TA instruments, New Castle, DE, USA). The mechanical property analysis was performed using conventional testing techniques such as pendulum hardness and scratch and impact resistance. Nanoindentation was utilized in order to check the influence of the nanoparticles on the hardness and modulus of the coatings, while the anticorrosion properties of the coatings by exposing them to a 3.5% NaCl solution were analyzed with the help of Electrochemical Impedance Spectroscopy (EIS, Metrohm, Amsterdam, The Netherland).

2. Materials and Methods

The coating was prepared using ZnO nanopowder for the formulations (E51–E55). These formulations are shown in Table 1. The formulations were prepared by utilizing epoxy resin of the bisphenol A type, the use of solvents Methyl Isobutyl Ketone (MIBK) and xylene in order to facilitate the mixing. An agent was also used to release the air trapped during the sample preparation. Before the addition of the ZnO nanoparticles into epoxy, the

nanoparticles were surface treated using silane. An equal proportion of both the silane and nanoparticles was mixed in acetone gradually for 5 h at 3000–5000 rpm. After mixing, the prepared solution was dried for 12–18 h at a temperature of 100 °C, and the dried powder was reground using a mechanical grinder. The treated particles were again dispersed for 2 h in acetone at 3000–5000 rpm. The final obtained solution was then added dropwise into the epoxy matrix in a span of 30 min at 3000–5000 rpm. This prepared slurry of the epoxy nanoparticles was placed in an oven at 100 °C for 1 h. The optimized hardener and the solvent were added into the nanoparticle incorporated epoxy resin at 1000 rpm. The hardener used had a relatively low viscosity and low-hydrogen-equivalent weight and was obtained from Huntsman Advanced Materials for it outstanding corrosion resistance and wet adhesion applications. The final reaction mixture was kept for 10 min for stabilization. The complete formulation ingredients and quantity used are listed in Table 1.

Table 1. Composition details of the prepared samples.

Code	Resin	ZnO	Xylene	MIBK	Air Release	Hardener
E51	82.91	0.5	30	30	1	16.57
E52	82.08	2.0	30	30	1	16.41
E53	80.83	3.0	30	30	1	16.16
E54	79.58	4.5	30	30	1	15.91
E55	78.33	6.0	30	30	1	15.66

The cross-linking was carried out at room temperature by mixing a stoichiometric quantity of epoxy with the polyamide hardener. All the epoxy coating samples were coated on glass plate and steel panel to test the mechanical and electrochemical properties. The coatings were left for curing for 7 days, and after completion of the curing, the obtained coating thickness after drying, termed as Dry Film Thickness (DFT), was measured with the help of Eco-test plus from Sheen Instruments (Surrey, UK). To analyze any changes in the chemical linkages, FTIR-ATR analysis was performed. The morphology of the prepared coatings and the dispersion of nanoparticles were observed with the help of Field Emission Scanning Electron Microscope (FE-SEM, JEOL, Tokyo, Japan). To check the thermal properties of the ZnO-incorporated epoxy coatings, Differential Scanning Calorimetry (DSC, TA instruments, New Castle, DE, USA) was performed. For the evaluation of the mechanical properties with increasing ZnO percentages, the pendulum hardness (Model: 707/K-ASTM D4366) was used for each coating on glass. At least five different readings were recorded at different points on the coated glass plates, and the average value is reported. Each time, the pointer oscillated in front of the sensor of the tester, and it counted the number of passes. This means that the number of oscillations increased with the increased hardness of the coatings. The resistance against scratches of the prepared coatings was observed with the help of the Sheen Automatic Scratch Tester (Surrey, UK, Model: 705, ASTM D-7027), in which the sample was mounted against a scratch probe facing the sample at 45° connected to a metal rod to support weights. The weights were changed gradually from 500 g to 10 Kg until the coating was completely marred. An impact test (BYK Model: IG-1120-ASTM D2794) was also performed to check the impact resistance of the coatings. The nanomechanical properties of the coatings were analyzed with the help of the Nanotest Platform from Micro Materials Ltd., Wrexham, UK. A Berkovich-type indenter was used for this purpose, and a load control program was used, where the coatings were forced against the indenter up to a maximum load of 10 mN. The loading rate for the coatings was kept at 0.1 mN/s, followed by a holding time of 60 s to negate the effect of creep, then the unloading was performed using a similar rate until the load was completely removed. At least 5 indentations were taken at different locations, and the average of the results is reported. In order to analyze the anticorrosion properties of the ZnO-incorporated epoxy, electrochemical impedance spectroscopy (Autolab Potentiostat, Metrohm, Amsterdam, The Netherlands) was used. The analysis was performed in 3.5% NaCl solutions with two different immersion time periods (1 h to 7 days). The analysis was conducted by applying

±5 mV amplitude sinusoidal wave perturbation in a frequency range between 100,000 and 0.1 Hz.

3. Results

3.1. Field Emission Scanning Electron Microscopy

The changes in the epoxy coatings' morphology after the addition of the nanoparticles in various percentages were investigated with the help of FESEM. The FESEM micrographs obtained for the blank epoxy and nanoparticle-reinforced samples are displayed in Figure 1 below. It can be seen in Figure 1a that the blank sample had a very smooth surface. With the addition of 0.5 wt.% ZnO, prominent visible white spots were observed all over the surface. Increasing the percentage of the nanoparticles to 2 wt.% (Figure 1b), the distribution of the nanoparticles was even throughout the sample. With a further increase in the nanoparticle percentage to 3 wt.%, 4.5 wt.%, and 6 wt.%, a clear agglomeration was visible across the coating surface, where the visible bright white spots could be witnessed all across the surface (Figure 1d–f). The nanoparticle dispersion, in particular at higher loadings, was a very difficult task. At higher percentages, it became extremely difficult to achieve a homogenous dispersion due to the higher particle–particle interactions. Similar types of results were also reported in the literature, where a higher loading of nanoparticle led to poor dispersion and higher agglomeration [26–28].

In order to analyze the particle distribution, EDX was performed on the coating with 2 wt.% nanoparticles at the same area where the SEM was performed. The elemental distribution obtained from the sample is shown in Figure 2. The coating consisted of a hydrocarbon chain, and for this reason, the presence of carbon was the highest in the sample. The added filler distribution can be seen in this figure, where the distribution of Zn can be seen throughout the tested surface.
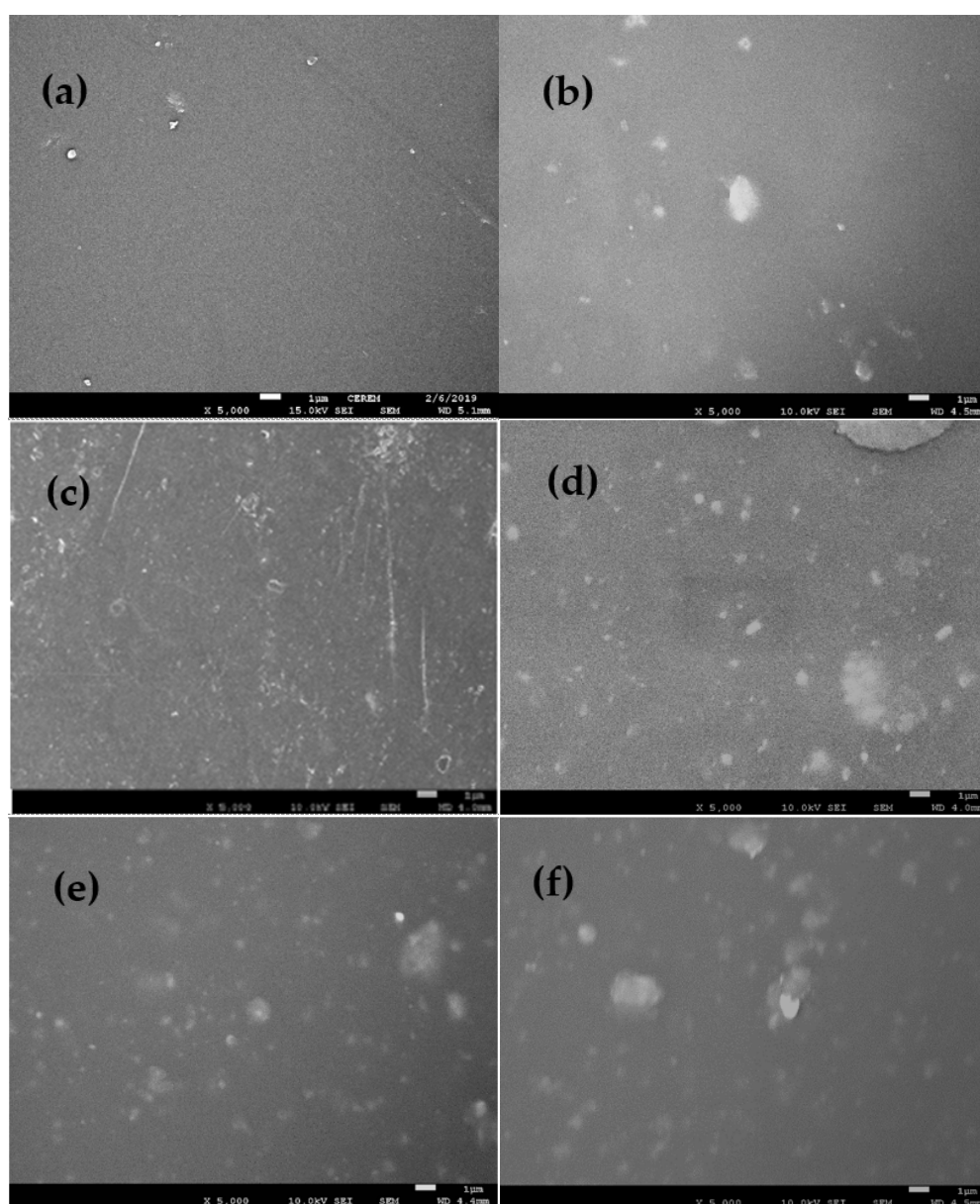
Figure 1. SEM images of (**a**) blank epoxy, (**b**) E51, (**c**) E52, (**d**) E53, (**e**) E54, and (**f**) E55.
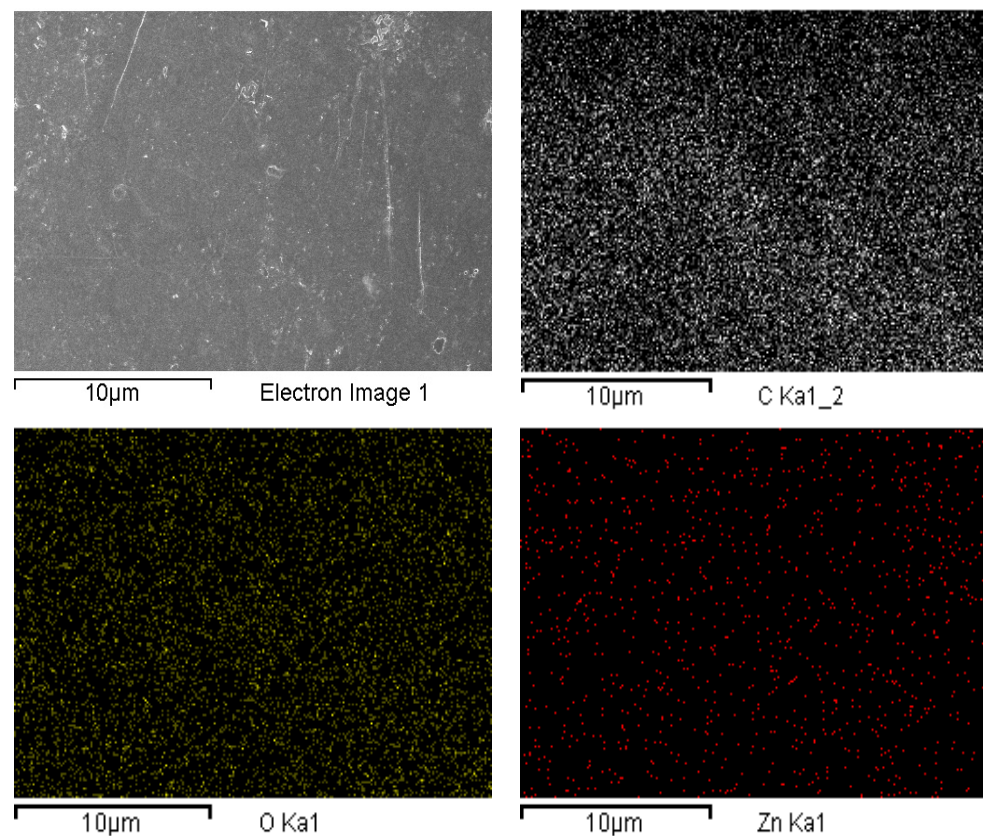
Figure 2. EDX mapping showing the particle distribution of the coatings containing 2 wt.% ZnO nanoparticles.

3.2. Fourier-Transformed Infrared Spectroscopy

To study the chemical composition of the epoxy coatings and the effects of nanoparticle addition on the curing behavior of the epoxy, FTIR analysis was performed. The scanning was performed in the range of 500–4000 cm^{-1} to obtain the FTIR spectrum. The DGEBA structure consisted of many organic groups. In order to focus on studying the curing behavior, the most important peaks corresponding to the curing of the epoxy and the hardener reaction with the addition of nanoparticles were 915 cm^{-1} (C–O vibration), NH_2 absorption vibration of the amine compound and OH stretching because of the epoxy cross-linking and ring opening (3340–3200 cm^{-1}), C–OH (3400–3500 cm^{-1}), CN group vibration (1109 cm^{-1}), and the epoxide ring (825 cm^{-1}). The FTIR results obtained for the nanoparticle-incorporated coatings are presented in Figure 3.
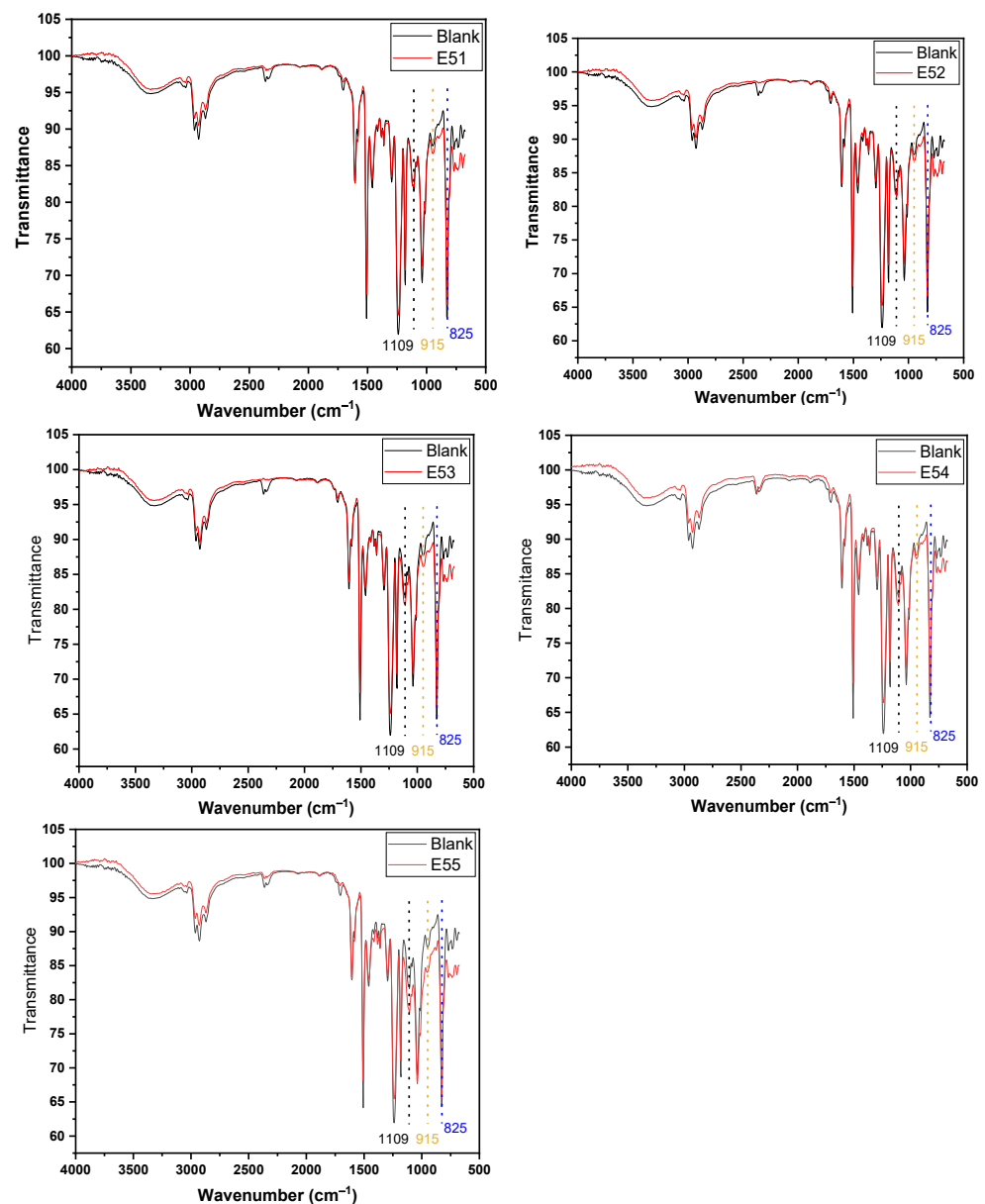
Figure 3. FTIR spectrum of blank and nanoparticle-incorporated coating samples in comparison.

The peak intensity at 915 cm^{-1}, which corresponds to the C–O vibrations of the epoxide group, were found to be 94 (blank), 95 (E51), 96 (E52), 96 (E53), 97 (E54), and 98 (E55). It was found that with increasing percentages of ZnO, the epoxy group vibration increased. The peak intensities at 1109 cm^{-1} were recorded as 82 (blank), 82 (E51), 81 (E52), 80 (E53), 80 (E54), and 78 (E55), which correspond to the CN vibration intensities. These CN vibration intensities represent the curing of the epoxy and hardener; the reduction in the intensities suggests a decrease in the curing of the coating with the increasing percentage of nanoparticles. Another confirmation of the decrease in curing with the nanoparticle addition corresponds to the peak intensity at 825 cm^{-1}. The intensities were recorded as 64 (blank), 66 (E51), 66 (E52), 67 (E53), 68 (E54), and 67 (E55), the increase in intensity with a higher nanoparticle percentage suggesting greater presence of the epoxide ring. Based on the evidence presented, it can be concluded that the presence of the nanoparticles in the system altered the curing behavior of the epoxy resin and hardener [26]. This effect was very small at lower percentages and very pronounced after a certain percentage followed by higher loadings.

3.3. Differential Scanning Calorimetry

The thermal characteristics such as the T_g of the prepared epoxy coatings with various percentages of ZnO nanoparticles were analyzed using differential scanning calorimetry. The DSC analysis indicated an enhancement in the glass transition temperature of the prepared coatings. The obtained values are provided in Table 2 with the ZnO powder-incorporated epoxy coating formulations. The highest value for the glass transition temperature was recorded for the coating with 2 wt.% of nanoparticles. With the increase in the loading of the nano-ZnO above 2 wt.%, the thermal properties were found to deteriorate. In all the prepared formulations, the coating with 2 wt.% of nanoparticles performed well because of the better nanoparticle–matrix interaction and the good dispersion of the nanoparticles. As also proven by FE-SEM, the increase in the percentage beyond 2 wt.% increased the particle–particle interaction, and the nanoparticles started to agglomerate considerably. This was supported by the findings that using 2 wt.% ZnO particles can increase the T_g of the nanocomposite. In addition, the incorporation of the nanoparticles affected the rheology of the coatings. The cross-linking density of the coating containing more than 2 wt.% of nano-ZnO decreased. The increase in the glass transition temperature was because of the strong physical bonding between the epoxy resin and the nanoparticles at lower loadings. However, at a higher loading of the nanoparticles, the decrease in the cross-linking density was due to incomplete curing of the composites in the presence of the nanoparticles [29] (already explained in Section 3.2).

Table 2. Glass transition temperature of the nanoparticle-incorporated coatings.

Code	T_g (°C)
E51	45.75
E52	53.31
E53	50.19
E54	49.66
E55	48.41

The T_g and cross-linking density of the coatings reinforced with 3 wt.%, 4.5 wt.%, and 6 wt.% of nanoparticles decreased. The decrease in the values of T_g and the cross-linking density were more pronounced at 6 wt.%. This revealed the greater hindrance effect of the nanoparticles on the curing behavior of the coating. The decrease in the T_g of the composites reinforced with 3 wt.% to 6 wt.% of nanoparticles can be attributed to the significant decrease in the cross-linking density of these coatings. The lowest T_g at 4.5 wt.% can be attributed to the higher influence of the agglomerated particles on the curing behavior of the coating [30].

3.4. Mechanical Properties and Nanoindentation

To study the effect of the nanoparticles on the mechanical properties of the prepared coatings, the samples were characterized with the help of pendulum hardness, scratch resistance, and impact strength. The results obtained for these tests are presented in Table 3. With the increasing percentage of nanoparticles, the pendulum hardness was also found to increase, which is an indication of increased surface hardness. The impact and scratch resistance of the prepared coatings were also evaluated. A sharp decline in both impact and scratch resistance was observed after the 2 wt.% addition of the nanoparticles, and the particle loadings beyond 2 wt.% influenced the coatings' properties negatively. With the increase in the ZnO percentage, a drastic decrease in both impact and scratch was witnessed, indicating the brittle nature of the prepared coatings with high ZnO loadings. This was due to the stiffness because of the nanoparticles, and the reason behind this stiffness was their agglomeration, which became increasingly difficult to disperse at higher loadings. The poor dispersion of the nanoparticles was already explained with the SEM images above. The agglomeration of the nanoparticles restricted the chain mobility in the

coating, as well as resulted in a slight crack in the coating because the localized stress due to agglomeration led to the deterioration of their properties.

Table 3. The obtained results for pendulum hardness and impact and scratch resistance.

Code	Dry Film Thickness (μm)	Pendulum Hardness (Oscillations)	Scratch Resistance (Kg)	Impact Resistance (lb/in^2)
E51	70–90	116	7.2	104
E52	70–90	125	8.5	112
E53	70–90	123	5.6	96
E54	70–90	124	5.3	80
E55	70–90	125	3.3	56

The nanomechanical properties of the prepared coatings such as the hardness and elastic modulus were analyzed with the help of the Nano Test Platform from Micromaterials (Wrexham, UK). The samples were analyzed with a load control program, using a Berkovich-type indenter. The prepared coatings were subjected to a maximum load of 10 mN at a loading rate of 0.1 mN/s. Upon reaching the maximum load, the samples were subjected to a holding time of 60 s to reduce the effect of creep because of the viscoelastic nature of polymers. After the holding period, the load was removed from the samples using the same rate of 0.1 mN/s until the load was completely removed. At least five indentations were made on each sample at different locations, and the average results are reported. Figure 4 below shows the load vs. depth profile of all the samples. The maximum penetration depths for the samples were 1310, 1281, 1427, 1302, and 1388 nm for E51, E52, E53, E54, and E55, respectively. The higher the depth penetration, the lower was the resistance of the coatings under the influence of the external load [31]. It can be seen that the lowest depth penetration was obtained for the coating sample with 2 wt.% of ZnO nanoparticles. Upon a further increase in the ZnO percentage, the load-bearing capacity of the coatings became poor. It can be seen in Figure 3 that, in particular, samples E54 and E55 showed that the loading was not smooth and showed some abrupt penetration abnormalities, which further confirmed that these coatings were not homogenous.
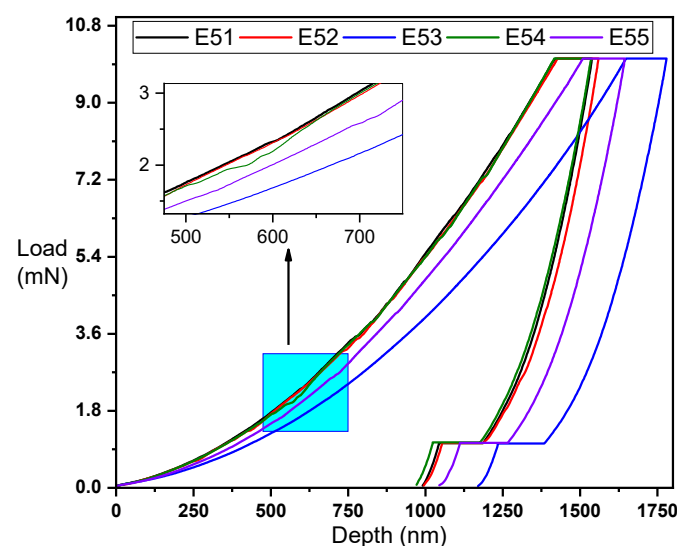

Figure 4. Load vs. depth profile of ZnO-incorporated epoxy coatings E51 (1%), E52 (2%), E53 (3%), E54 (4%), and E55 (5%).

After the experimentation process, all the obtained graphs were analyzed with the help of the inbuilt machine software in order to extract the hardness and modulus of elasticity of the prepared samples. The analysis was performed using the Oliver and Pharr

method [32,33] for the extraction of the results. The hardness and modulus results were obtained using the following equations.

$$H = Fmax/Ac \tag{1}$$

$$1/Er = (1 - v^2)/E + (1 - vi^2)/Ei \tag{2}$$

where H = hardness, Fmax = max applied load, Ac = projected area of contact, Er = reduced modulus, v and vi the Poisson ratios of the sample (0.35 for the polymer) and diamond indenter (0.07), and E and Ei the elastic modulus of the sample (obtained from Equation (2)) and the diamond indenter (1141 GPa) [34].

Table 4 presents the values obtained for the hardness and elastic modulus for the prepared coatings. It can be seen that with the addition of 0.5 wt.% and 2 wt.% of ZnO nanoparticles, an increase in the hardness and modulus was witnessed, whereas with the further increase of the nanoparticles percentage to 3 wt.%, 4.5 wt.%, and 6 wt.%, the obtained values were lower than the value obtained for the 2 wt.% nanoparticle content. This increase in hardness and modulus was because of the nanoparticle addition. The epoxy structure possessed a free volume because of the polymer chain entanglement and cross-linking. The addition of nanoparticles filled up this free volume between the polymer chains and made the material stiff, which increased the hardness due to the restricted chain movement.

Table 4. Hardness and modulus values of the ZnO-modified epoxy coatings.

Sample	Hardness (GPa)	Modulus (GPa)
E51	0.213 ± 0.002	4.560 ± 0.056
E52	0.225 ± 0.004	4.818 ± 0.039
E53	0.185 ± 0.009	4.935 ± 0.046
E54	0.218 ± 0.013	4.603 ± 0.102
E55	0.191 ± 0.010	4.119 ± 0.098

At higher loading of the nanoparticles, the agglomeration of the particles (described in Section 1) was the main reason behind this decrease in the properties of the coatings. The non-uniform loading behavior itself suggested that the coating was not homogenous and the indenter while testing landed at an area with nanoparticle agglomeration, which after reaching a certain load, abruptly penetrated in the coating. This behavior could be clearly witnessed throughout the loading cycle until the maximum load was achieved.

The obtained nanoindentation results were in compliance with the conventional mechanical testing results. The increase in pendulum hardness at higher loading was certainly because of the surface stiffness with the particle agglomeration, since this technique gives the information about the surface stiffness. On the other hand, the other tests that predicted the bulk properties of the coatings such as the impact and scratch suggested that an increase in the nanoparticle percentage resulted in a reduction of the coating properties. The scratch and impact properties reduced significantly with increasing percentages after 2 wt.% of nanoparticle loading [29,35].

3.5. Electrochemical Impedance Spectroscopy

Electrochemical Impedance Spectroscopy (EIS) is a non-destructive technique that enables studying the corrosion protection mechanism of coatings. Furthermore, EIS is a sensitive technique that can pick up coating degradation prior to its visual manifestation [36–38]. The anticorrosive performance of the epoxy coating system (E51–E55) was monitored using EIS in a classic three-electrode cell. EIS measurements were performed using a potentiostat/galvanostat (Auto lab Ecochemie PGSTAT 30, Metrohm, Amsterdam, Netherland) equipped with a FRA2 frequency response analyzer module. Frequency scans were carried out by applying a ±5 mV amplitude sinusoidal wave perturbation. The analyzed frequency range was from 100 kHz to 1 MHz, and the electrolyte used was a 3.5%

NaCl solution. The impedance spectra for the epoxy coatings were obtained with exposure of 1 h and after a time interval of 7 days of the immersion in the 3.5% NaCl solution. The interpretation of the impedance data was performed using the Autolab Frequency Response Analyser (FRA, NOVA 1.8) software. The obtained Nyquist plots for 1 h and 7 days of exposure are presented in Figures 5 and 6.
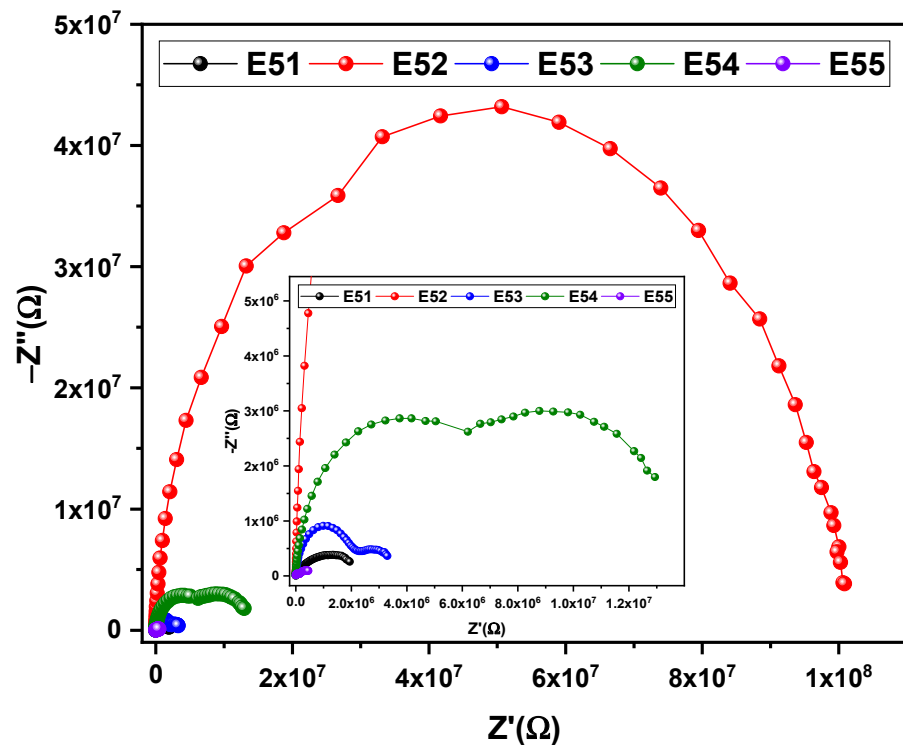

Figure 5. Obtained Nyquist plots for the nano-ZnO-incorporated coatings after 1 h of exposure.
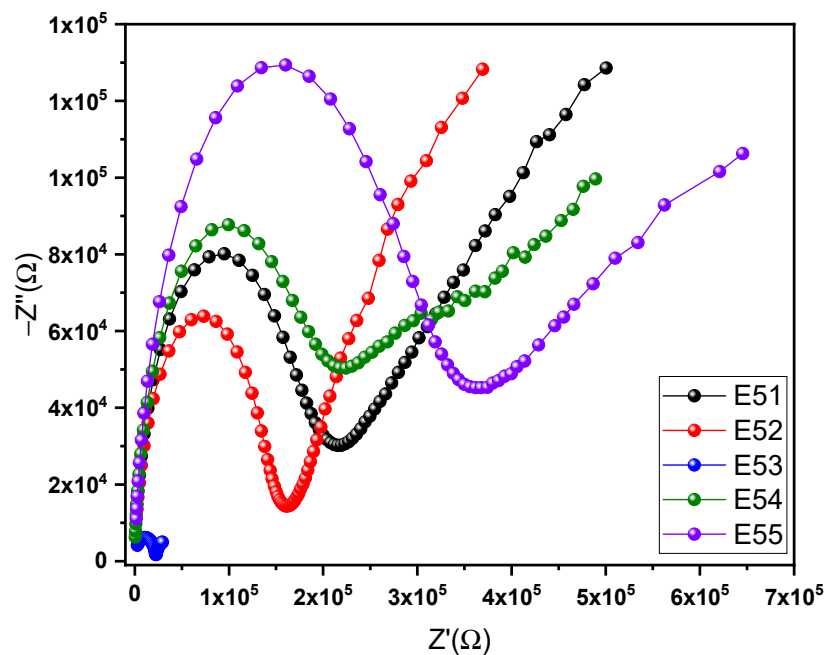

Figure 6. Obtained Nyquist plots for the nano-ZnO-incorporated coatings after 7 days of exposure.

Electrochemical impedance spectroscopy of the coated steel specimens obtained during exposure to the aerated 3.5 wt.% NaCl aqueous solution was performed for the selected

exposure times of 1 h and 7 days. The Nyquist plots showed two time constant semicircles for all the coatings containing nanoparticles after exposure of 1 h except the E52 sample, where a single semicircle was obtained. The semicircle is an indication of a compact coating. After the exposure of 7 days in the chloride solution, a second time constant was obtained, which was detected as a second semicircle in the Nyquist plots of all the coating samples. This means that the corrosive electrolyte penetrated into the coating interface in a very short immersion time [39]. In order to obtain the correct information regarding the coating performance when exposed to the electrolyte solution, the obtained Nyquist data were fit using the electrochemical model shown in Figure 7, where R is the solution resistance, R_{P1} is the coating resistance (assuming coatings contain pores), Q_1 is a constant phase element, R_{P2} is the charge transfer resistance, Q_2 is a second constant phase element. The values obtained for these parameters are reported in Table 5. The R_{P1} corresponds to the resistance between the epoxy coating surface and the electrolyte solution, which was assumed to be of a porous nature. In the following circuit, both R_{P1} and R_{P2} are connected in series; hence, the polarization resistance is equivalent to the sum of both resistances [40–42].
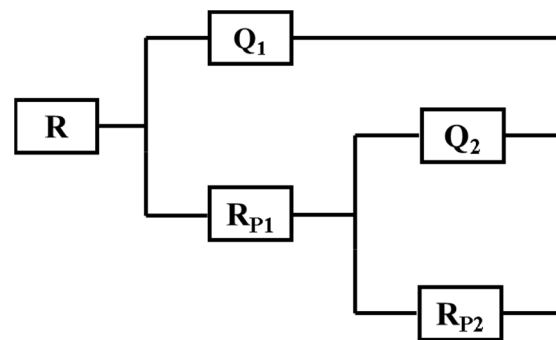

Figure 7. Equivalent circuit model used to fit the EIS data.

Table 5. Obtained parameters after fitting samples to the 3.5% NaCl solution.

Sample	R_s (Ω)	R_{P1} (kΩ)	CPE (Q_1)		R_{P2} (kΩ)	CPE (Q_2)	
			nMho	n		nMho	n
E51 (1-h)	559	85.8	0.77	0.96	2350	230	0.40
E51 (7-D)	781	161	2.29	0.90	2110	501	0.26
E52 (1-h)	19.8	70300	1.78	0.98	32600	10.8	0.62
E52 (7-D)	810	145	2.80	0.93	3530	111	0.40
E53 (1-h)	202	1870	2.08	0.94	2060	338	0.51
E53 (7-D)	209	25.6	2.20	0.57	120	491	0.81
E54 (1-h)	170	4350	3.45	0.96	11500	80.4	0.51
E54 (7-D)	90.6	134	3.48	0.90	810	255	0.27
E55 (1-h)	201	77.1	2.79	0.93	610	187	0.38
E55 (7-D)	445	259	3.23	0.89	960	348	0.26

The value of R_{P1} decreased with the increase of the exposure time, and this happened because of the defects in the coatings, which caused the penetration of the electrolyte. R_{P2} is the resistance at the coating metal interphase (also known as charge transfer resistance), which is indicative of corrosion product formation at the coating metal interphase when water penetrates towards the substrate. As can be seen from Table 5, the higher values of R_{P1} and R_{P2} were obtained for the coatings with 2 wt.% of ZnO (E52). This was because of the higher dispersion achieved, which produced a compact coating surface with minimal defects. With the increase in the percentage of ZnO, the anticorrosion properties of the coatings deteriorated because of the poor dispersion, which caused the defects in the coatings, which means that the dispersion of the nanoparticles played a vital role in the

corrosion protection properties of the coatings. The poor dispersion caused agglomeration in the coating, which led to the formation of defects in the coating surface. These defects became the pathways for the diffusion of the electrolyte, ultimately reaching the metal coating interface, causing the corrosion of the metal.

With the increase of the exposure time to 7 days, two time constants appeared for all the coating samples. The appearance of two time constant corresponded to the diffusion of the electrolyte at the coating–metal interface, which caused the corrosion of the substrate underneath the coating [39]. The obtained values after fitting with the model presented in Table 5 suggest a drastic decrease in both R_{P1} and R_{P2} for all the coatings. Even after diffusion, the coating with 2 wt.% of ZnO proved to be the best followed by the coating with 1 wt.% of ZnO in comparison to the other coatings. It is worth noting that the increase in the nanoparticle percentage beyond 2 wt.% caused a drastic decrease in the anticorrosion performance of the coatings. It may be observed that with the increase in the immersion time, the coating capacitance values decreased depending on the water content in the coatings, the lowest decrease in the coating capacitance being observed for the coating with 2 wt.% of nanoparticles.

4. Conclusions

The influence of ZnO nanoparticle percentage was studied in this research. The prepared coatings samples were subjected to FTIR, FE-SEM, thermal, nanomechanical, and electrochemical characterizations. The FE-SEM images revealed that the dispersion of the nanoparticles was a very challenging task, especially at higher loading levels. At a higher percentage of loading, the nanoparticles agglomerated heavily because of the greater internal forces of attraction. The FTIR results revealed that the addition of nanoparticles in the epoxy/hardener system affected the curing behavior of the coatings. It was found that a higher nanoparticle content hindered the curing of the coatings. The thermal investigations revealed that the higher nanoparticle content caused a reduction in the cross-link density of the epoxy (which was confirmed by the FTIR with the decrease in the percent of curing), and this caused a reduction in the T_g of the coatings because of the reduced cross-link density. The mechanical and nanoindentation analysis also suggested inferior coating properties at higher nanoparticle loadings. The anticorrosion properties were also greatly influenced with the addition of the ZnO nanoparticles. The conclusive results from all the characterizations suggested that the addition of 2 wt.% of nanoparticles outperformed all the other loadings and showed the best performance.

Author Contributions: Conceptualization, M.A.A.; methodology, M.A.A.; Investigation, M.A.A., U.A.S., H.S.A. and A.A.; formal analysis, M.A.A., U.A.S., A.A., H.S. and H.S.A.; writing—original draft preparation, U.A.S.; writing—review and editing, U.A.S., M.A.A., A.A., H.S., H.S.A. and S.M.A.-Z.; supervision, S.M.A.-Z.; project administration, S.M.A.-Z. All authors have read and agreed to the published version of the manuscript.

Institutional Review Board Statement: Not applicable.

Informed Consent Statement: Not applicable.

Data Availability Statement: Data is contained within the article.

Conflicts of Interest: The authors declare no conflict of interest.

References

1. Chandrasekaran, S. *Electrodeposition of Bis-Silane for the Pretreatment of Aluminum Alloys*; University of Cincinnati: Cincinnati, OH, USA, 2006.
2. Zand, B.N.; Mahdavian, M. Corrosion and adhesion study of polyurethane coating on silane pretreated aluminum. *Surf. Coat. Tech.* **2009**, *203*, 1677–1681. [CrossRef]
3. May, C. *Epoxy Resins: Chemistry and Technology*; Routledge: Abingdon, UK, 2018.

4. Mailhot, N.; Morlat-Theias, S.; Ouahioune, M.; Gardette, J.L. Study of the degradation of an epoxy/amine resin, 1 photo- and thermo-chemical mechanisms. *Macromol. Chem. Physic.* **2005**, *206*, 575–584. [CrossRef]
5. Razin, A.A.; Yari, H.; Ramezanzadeh, B. Stone-chipping and adhesion deterioration of automotive coating systems caused by outdoor weathering of underneath layers. *J. Ind. Eng. Chem.* **2015**, *31*, 291–300. [CrossRef]
6. Liu, J.M.; Yang, S.C. Novel colloidal polyaniline fibrils made by template guided chemical polymerization. *J. Chem. Soc. Chem. Comm.* **1991**, 1529–1531. [CrossRef]
7. Alexandre, M.; Dubois, P. Polymer-layered silicate nanocomposites: Preparation, properties and uses of a new class of materials. *Mat. Sci. Eng. R* **2000**, *28*, 1–63. [CrossRef]
8. Chaiko, D.J.; Leyva, A.A. Thermal transitions and barrier properties of olefinic nanocomposites. *Chem. Mater.* **2005**, *17*, 13–19. [CrossRef]
9. Sabzi, M.; Mirabedini, S.M.; Zohuriaan-Mehr, J.; Atai, M. Surface modification of TiO_2 nano-particles with silane coupling agent and investigation of its effect on the properties of polyurethane composite coating. *Prog. Org. Coat.* **2009**, *65*, 222–228. [CrossRef]
10. Rashvand, M.; Ranjbar, Z.; Rastegar, S. Nano zinc oxide as a UV-stabilizer for aromatic polyurethane coatings. *Prog. Org. Coat.* **2011**, *71*, 362–368. [CrossRef]
11. Aloui, F.; Ahajji, A.; Irmouli, Y.; George, B.; Charrier, B.; Merlin, A. Inorganic UV absorbers for the photostabilisation of wood-clearcoating systems: Comparison with organic UV absorbers. *Appl. Surf. Sci.* **2007**, *253*, 3737–3745. [CrossRef]
12. Allen, N.S.; Edge, M.; Ortega, A.; Liauw, C.M.; Stratton, J.; McIntyre, R.B. Behaviour of nanoparticle (ultrafine) titanium dioxide pigments and stabilisers on the photooxidative stability of water based acrylic and isocyanate based acrylic coatings. *Polym. Degrad. Stabil.* **2002**, *78*, 467–478. [CrossRef]
13. Ranjbar, Z.; Ashhari, S.; Jannesari, A.; Montazeri, S. Effects of nano silica on the Anticorrosive properties of epoxy coatings. *Prog. Color Color. Coat.* **2013**, *6*, 119–128.
14. Panek, M.; Hysek, S.; Dvorak, O.; Zeidler, A.; Oberhofnerova, E.; Simunkova, K.; Sedivka, P. Durability of the exterior transparent coatings on nano-photostabilized english oak wood and possibility of its prediction before artificial accelerated weathering. *Nanomaterials* **2019**, *9*, 1568. [CrossRef] [PubMed]
15. Bui, T.M.A.; Nguyen, T.V.; Nguyen, T.M.; Hoang, T.H.; Nguyen, T.T.H.; Lai, T.H.; Tran, T.N.; Nguyen, V.H.; Hoang, V.H.; Le, T.L.; et al. Investigation of crosslinking, mechanical properties and weathering stability of acrylic polyurethane coating reinforced by SiO_2 nanoparticles issued from rice husk ash. *Mater Chem. Phys.* **2020**, *241*, 122445. [CrossRef]
16. Saadat-Monfared, A.; Mohseni, M. Polyurethane nanocomposite films containing nano-cerium oxide as UV absorber; Part 2: Structural and mechanical studies upon UV exposure. *Colloid Surface A* **2014**, *441*, 752–757. [CrossRef]
17. Amrollahi, S.; Ramezanzadeh, B.; Yari, H.; Ramezanzadeh, M.; Mahdavian, M. In-situ growth of ceria nanoparticles on graphene oxide nanoplatelets to be used as a multifunctional (UV shield/radical scavenger/anticorrosive) hybrid compound for exterior coatings. *Prog. Org. Coat.* **2019**, *136*, 105241. [CrossRef]
18. Pakravan, H.R.; Yari, H. The influence of nanostructured UV-blockers on mechanical properties of carbon fiber epoxy composites during accelerated weathering condition. *Polym. Adv. Technol.* **2018**, *29*, 970–981. [CrossRef]
19. Rasouli, D.; Dintcheva, N.T.; Faezipour, M.; La Mantia, F.P.; Farahani, M.R.M.; Tajvidi, M. Effect of nano zinc oxide as UV stabilizer on the weathering performance of wood-polyethylene composite. *Polym. Degrad. Stabil.* **2016**, *133*, 85–91. [CrossRef]
20. Haniffa, M.A.M.; Ching, Y.C.; Chuah, C.H.; Ching, K.Y.; Liou, N.S. Synergistic effect of (3-Aminopropyl)Trimethoxysilane treated ZnO and corundum nanoparticles under UV-irradiation on UV-cutoff and IR-absorption spectra of acrylic polyurethane based nanocomposite coating. *Polym. Degrad. Stabil.* **2019**, *159*, 205–216. [CrossRef]
21. Eren, M.; Can, H.K. Preparation of zinc methacrylate-methylmethacrylate-butyl acrylate emulsions and their application in exterior paints. *Prog. Org. Coat.* **2019**, *135*, 424–437. [CrossRef]
22. Ashassi-Sorkhabi, H.; Seifzadeh, D.; Raghibi-Boroujeni, M. Analysis of electrochemical noise data in both time and frequency domains to evaluate the effect of ZnO nanopowder addition on the corrosion protection performance of epoxy coatings. *Arab. J. Chem.* **2016**, *9*, S1320–S1327. [CrossRef]
23. Ammar, S.; Ramesh, K.; Vengadaesvaran, B.; Ramesh, S.; Arof, A.K. Amelioration of anticorrosion and hydrophobic properties of epoxy/PDMS composite coatings containing nano ZnO particles. *Prog. Org. Coat.* **2016**, *92*, 54–65. [CrossRef]
24. Parimalam, M.; Islam, M.R.; Yunus, R.M. Effects of nanosilica, zinc oxide, titatinum oxide on the performance of epoxy hybrid nanocoating in presence of rubber latex. *Polym. Test* **2018**, *70*, 197–207. [CrossRef]
25. Xiong, M.; Gu, G.; You, B.; Wu, L. Preparation and characterization of poly (styrene butylacrylate) latex/nano-ZnO nanocomposites. *J. Appl. Polym. Sci.* **2003**, *90*, 1923–1931. [CrossRef]
26. Ramezanzadeh, B.; Attar, M.M.; Farzam, M. Effect of ZnO nanoparticles on the thermal and mechanical properties of epoxy-based nanocomposite. *J. Therm. Anal. Calorim.* **2011**, *103*, 731–739. [CrossRef]
27. Ramezanzadeh, B.; Attar, M.M. Studying the corrosion resistance and hydrolytic degradation of an epoxy coating containing ZnO nanoparticles. *Mater. Chem. Phys.* **2011**, *130*, 1208–1219. [CrossRef]
28. Ramezanzadeh, B.; Attar, M.; Farzam, M. A study on the anticorrosion performance of the epoxy–polyamide nanocomposites containing ZnO nanoparticles. *Prog. Org. Coat.* **2011**, *72*, 410–422. [CrossRef]
29. Shi, X.M.; Nguyen, T.A.; Suo, Z.Y.; Liu, Y.J.; Avci, R. Effect of nanoparticles on the anticorrosion and mechanical properties of epoxy coating. *Surf. Coat. Tech.* **2009**, *204*, 237–245. [CrossRef]

30. Shi, H.W.; Liu, F.C.; Yang, L.H.; Han, E.H. Characterization of protective performance of epoxy reinforced with nanometer-sized TiO_2 and SiO_2. *Prog. Org. Coat.* **2008**, *62*, 359–368. [CrossRef]

31. Alam, M.A.; Samad, U.A.; Alam, M.; Anis, A.; Al-Zahrani, S.M. Enhancement in nanomechanical, thermal, and abrasion properties of SiO_2 nanoparticle-modified epoxy coatings. *Coatings* **2020**, *10*, 310. [CrossRef]

32. Oliver, W.C.; Pharr, G.M. An improved technique for determining hardness and elastic-modulus using load and displacement sensing indentation experiments. *J. Mater. Res.* **1992**, *7*, 1564–1583. [CrossRef]

33. Oliver, W.C.; Pharr, G.M. Measurement of hardness and elastic modulus by instrumented indentation: Advances in understanding and refinements to methodology. *J. Mater. Res.* **2004**, *19*, 3–20. [CrossRef]

34. Alam, M.A.; Samad, U.A.; Sherif, E.S.M.; Alothman, O.; Seikh, A.H.; Al-Zahrani, S.M. Effects of minor additions of polypyrrole on the thermal, mechanical and electrochemical properties of epoxy-2pack coatings. *Int. J. Electrochem. Sci.* **2017**, *12*, 74–89. [CrossRef]

35. Samad, U.A.; Alam, M.A.; Chafidz, A.; Al-Zahrani, S.M.; Alharthi, N.H. Enhancing mechanical properties of epoxy/polyaniline coating with addition of ZnO nanoparticles: Nanoindentation characterization. *Prog. Org. Coat.* **2018**, *119*, 109–115. [CrossRef]

36. Abdus Samad, U.; Alam, M.A.; Sherif, E.-S.M.; Alam, M.; Shaikh, H.; Alharthi, N.H.; Al-Zahrani, S.M. Synergistic effect of Ag and ZnO nanoparticles on polypyrrole-incorporated epoxy/2pack coatings and their corrosion performances in chloride solutions. *Coatings* **2019**, *9*, 287. [CrossRef]

37. Alam, M.A.; Samad, U.A.; Sherif, E.M.; Seikh, A.; Al-Zahrani, S.M.; Alharthi, N.H.; Alam, M. Synergistic effect of Ag and ZnO nanoparticles on polyaniline incorporated epoxy/2pack coatings for splash zone applications. *J. Coat. Technol. Res.* **2019**, *16*, 835–845. [CrossRef]

38. Abdus Samad, U.; Alam, M.A.; Anis, A.; Sherif, E.M.; Al-Mayman, S.I.; Al-Zahrani, S.M. Effect of incorporated zno nanoparticles on the corrosion performance of SiO_2 nanoparticle-based mechanically robust epoxy coatings. *Materials* **2020**, *13*, 3767. [CrossRef]

39. Kumar, S.A.; Sasikumar, A. Studies on novel silicone/phosphorus/sulphur containing nano-hybrid epoxy anticorrosive and antifouling coatings. *Prog. Org. Coat.* **2010**, *68*, 189–200. [CrossRef]

40. Zeybek, B.; Pekmez, N.O.; Kilic, E. Electrochemical synthesis of bilayer coatings of poly(N-methylaniline) and polypyrrole on mild steel and their corrosion protection performances. *Electrochim. Acta* **2011**, *56*, 9277–9286. [CrossRef]

41. Yalçınkaya, S.; Tüken, T.; Yazıcı, B.; Erbil, M. Electrochemical synthesis and corrosion behaviour of poly (pyrrole-co-o-anisidine-co-o-toluidine). *Curr. Appl. Phys.* **2010**, *10*, 783–789. [CrossRef]

42. Chaudhari, S.; Patil, P.P. Inhibition of nickel coated mild steel corrosion by electrosynthesized polyaniline coatings. *Electrochim. Acta* **2011**, *56*, 3049–3059. [CrossRef]